

# Conformation of glycosaminoglycans by ion mobility mass spectrometry and molecular modelling†

Lan Jin,<sup>a</sup> Perdita E. Barran,<sup>a</sup> Jon A. Deakin,<sup>b</sup> Malcolm Lyon<sup>b</sup> and Dušan Uhrín<sup>\*a</sup>

<sup>a</sup> University of Edinburgh, School of Chemistry, Joseph Black Building, West Mains Rd., Edinburgh, UK EH9 3JJ

<sup>b</sup> Cancer Research UK Department of Medical Oncology, University of Manchester, Christie Hospital NHS Trust, Wilmslow Road, Manchester, UK M20 4BX

Received 17th June 2005, Accepted 4th August 2005

First published as an Advance Article on the web 22nd August 2005

We have performed conformational analyses of heparin-derived oligosaccharide ions in the gas phase using a combination of ion-mobility mass spectrometry and molecular modelling. Negative mode electrospray ionisation was used to generate singly (disaccharide,  $[\text{C}_{12}\text{H}_{15}\text{NO}_{19}\text{S}_3\text{Na}_3]^-$ ) and doubly charged (tetrasaccharides,  $[\text{C}_{24}\text{H}_{30}\text{N}_2\text{O}_{38}\text{S}_6\text{Na}_6]^{2-}$  and  $[\text{C}_{24}\text{H}_{31}\text{N}_2\text{O}_{35}\text{S}_5\text{Na}_5]^{2-}$ ) ions containing three and six  $\text{Na}^+$  ions, respectively. Good agreement was obtained between the experimental and theoretical cross sections. The latter were obtained using modelled structures generated by the AMBER-based force field. Analysis of the conformations of the oligosaccharide ions shows that sodium cations play a major role in stabilizing these ions in the gas phase. This was seen in the formation of oligomers of the disaccharide ion and “compact” structures of tetrasaccharide ions. Interestingly, the gas phase conformations of the three tetrasaccharide ions with different primary structures were significantly different.

## 1. Introduction

Glycosaminoglycans (GAGs) are mostly linear polysaccharides found almost ubiquitously on animal cell surfaces and within extracellular matrices. They constitute an important class of biologically active macromolecules.<sup>1–3</sup> The most studied members of the GAG family are heparin and heparan sulfate (HS). HS and heparin initially share the same basic carbohydrate skeleton of a repeating disaccharide unit comprised of alternating  $\beta$ 1–4 linked glucuronic acid (GlcA) and  $\alpha$ 1–4 linked *N*-acetylglucosamine (GlcNAc) residues (Fig. 1a). Their subsequent structural differentiation results from the differing extents to which the post-polymeric enzymic modifications (*i.e.* GlcA epimerisation to iduronic acid (IdoA), and sulfations at various N- and O-positions), take place.<sup>4,5</sup> Within the highly sulfated domains of HS, short oligosaccharide sequences occur that are essentially identical to those commonly found in heparin. Such species can therefore be considered to be heparin/HS oligosaccharides.

More than a hundred proteins are known to bind to heparin *in vitro*<sup>6</sup> nevertheless, the physiologically relevant ligand in most cases will be HS, which is far more widely distributed. Information about the nature of these complexes comes from a limited number of X-ray structures.<sup>7</sup> Almost exclusively, these studies exploited fully sulfated heparin-derived oligosaccharides which form helical structures similar to those found in heparin fibres, as revealed by X-ray diffraction studies,<sup>8</sup> and in solution, as shown by NMR.<sup>9</sup> Nevertheless, models of HS–protein complexes, supported by biophysical and biochemical data, are emerging that involve longer glycan segments.<sup>10,11</sup> Inevitably, deviation from helical conformations of fully sulfated heparin must occur in order to accommodate such modes of binding. It is widely expected that this increased flexibility

will be associated with less sulfated regions of HS,<sup>12</sup> though little experimental evidence is available to support this supposition. Methodological advances in mapping the conformational space available to HS are therefore of considerable interest. Towards this end we have employed ion-mobility mass spectrometry (IM-MS) in combination with molecular modelling as a novel approach to probe the conformation of a series of highly sulfated HS/heparin oligosaccharides (Fig. 1b).

Ions drifting under the influence of a weak electrostatic field are retarded by collisions with a low pressure buffer gas. As a consequence, species with different overall shapes, or more specifically different rotationally averaged collision cross sections, are separated in time. This forms the basis for the conformational analysis by IM-MS, which, when used in conjunction with electrospray ionisation, has been applied to the study of various biomolecules, including peptides, proteins, and DNA.<sup>13,14</sup> Work of this nature does invariably meet opposition from an audience more used to solution-based structural studies. However, recent studies have indicated that, under certain conditions, solution conformations can be retained in the gas phase. This may be attributable to the gentle native electrospray ionisation conditions,<sup>15</sup> or may be a feature of the dominance of electrostatic interactions in a solution structure, which are then strengthened in the gas phase. This latter consequence has been illustrated by Gidden *et al.*,<sup>16</sup> who have used IM-MS in conjunction with molecular modelling to explore the persistence of DNA helices in the gas-phase.

Several other researchers have investigated the structures of HS species with mass spectrometry, but focusing on primary structure determination.<sup>17–21</sup> Gas-phase fragmentation, used in concert with enzymatic degradation and even <sup>2</sup>H and <sup>18</sup>O labelling, has successfully been employed to illustrate a mass spectrometry-based identification strategy for very complex mixtures of what are often isobaric species.<sup>22–24</sup> In contrast, we have exploited a different methodology here, which aims to determine the three-dimensional structure of GAG ions in the gas phase. If used in conjunction with higher-resolution

† Electronic supplementary information (ESI) available: Preparation of heparin-derived oligosaccharides. Colour images of Figures 4–6 are available in the HTML version. See <http://dx.doi.org/10.1039/b508644b>

IM-MS instrumentation,<sup>25–26</sup> it is possible that our approach could be used, in an analogous fashion to liquid chromatography separation, to distinguish the isomers present in a mixture, but in this case by virtue of their differing collision cross sections. This approach determines conformations using relatively low amounts of sample, and also could be used for analysis of mixtures, which is attractive given the practical difficulties associated with isolating pure HS species.

## 2. Materials and methods

Heparin-derived oligosaccharides (Fig. 1b) used in our study were prepared by enzymatic digestion of low molecular weight heparin. Details of this procedure are provided in the ESI†.

### NMR spectroscopy

The structures of oligosaccharides I–IV were confirmed by NMR spectroscopy using a 600 MHz Bruker Avance spectrometer equipped with a z-gradient triple-resonance cryoprobe. Samples containing 50 µg of oligosaccharides were dissolved in 320 µl of D<sub>2</sub>O and the spectra were acquired at 25 °C. The <sup>1</sup>H resonances of individual monosaccharide rings were assigned on the basis of 2D <sup>1</sup>H–<sup>1</sup>H TOCSY spectra. In the case of compound III, 2D ROESY spectra were also acquired. These latter spectra were used to identify the position of the missing sulfate in III. The proton chemical shifts of all oligosaccharides were in agreement with the published data for the same species,<sup>27</sup> although some differences, probably due to differences in pH, were observed.

### Ion mobility mass spectrometry

Gas-phase collision cross sections of oligosaccharides I–IV were determined using an Ion Mobility Mass Spectrometer

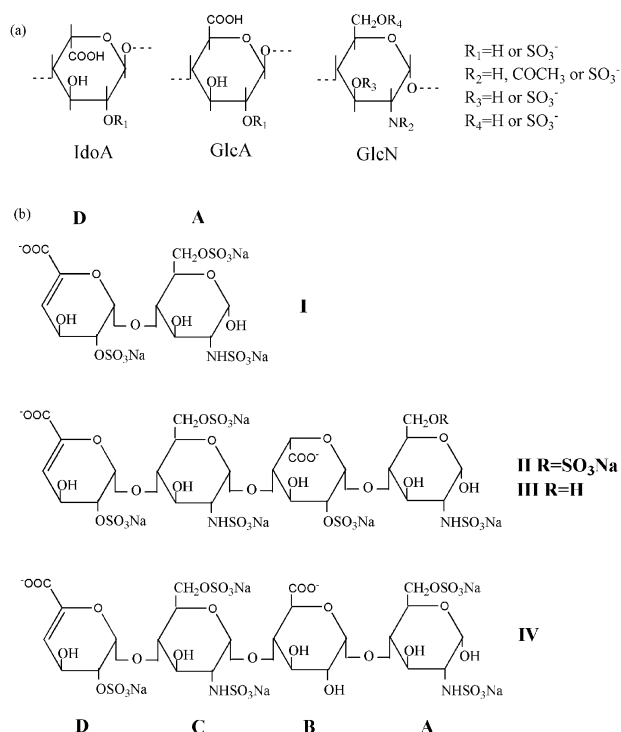


**Fig. 1** (a) Monosaccharide units of heparin/HS. (b) Structures of the heparin-derived disaccharide (I) and three tetrasaccharides (II–IV) used in this study. ΔUA(2S)-GlcNS(6S)-Na<sub>3</sub> (I), ΔUA(2S)-GlcNS(6S)-IdoA(2S)-GlcNS(6S)-Na<sub>6</sub> (II), ΔUA(2S)-GlcNS(6S)-IdoA(2S)-GlcNS-Na<sub>6</sub> (III) and ΔUA(2S)-GlcNS(6S)-GlcA-GlcNS(6S)-Na<sub>5</sub> (IV). Letters A–D are used to label individual rings starting from the reducing end (A) and progressing to the unsaturated non-reducing end (D) of the oligosaccharide.

**Table 1** Major peaks observed in mass spectra of oligosaccharides I–IV

Compound	Observed	Calculated	Assigned species
I	642.7	642.4	[C <sub>12</sub> H <sub>15</sub> NO <sub>19</sub> S <sub>3</sub> Na <sub>3</sub> ] <sup>-</sup>
	631.3	630.9	[C <sub>24</sub> H <sub>31</sub> N <sub>2</sub> O <sub>38</sub> S <sub>6</sub> Na <sub>5</sub> ] <sup>2-</sup>
	620.6	619.9	[C <sub>12</sub> H <sub>16</sub> NO <sub>19</sub> S <sub>3</sub> Na <sub>2</sub> ] <sup>-</sup>
II	642.8	642.4	[C <sub>24</sub> H <sub>30</sub> N <sub>2</sub> O <sub>38</sub> S <sub>6</sub> Na <sub>6</sub> ] <sup>2-</sup>
	631.6	630.9	[C <sub>24</sub> H <sub>31</sub> N <sub>2</sub> O <sub>38</sub> S <sub>6</sub> Na <sub>5</sub> ] <sup>2-</sup>
	621.1	620.4	[C <sub>24</sub> H <sub>32</sub> N <sub>2</sub> O <sub>38</sub> S <sub>6</sub> Na <sub>4</sub> ] <sup>2-</sup>
III	592.3	591.4	[C <sub>24</sub> H <sub>31</sub> N <sub>2</sub> O <sub>35</sub> S <sub>5</sub> Na <sub>5</sub> ] <sup>2-</sup>
	581.2	580.4	[C <sub>24</sub> H <sub>32</sub> N <sub>2</sub> O <sub>35</sub> S <sub>5</sub> Na <sub>4</sub> ] <sup>2-</sup>
	570.1	569.4	[C <sub>24</sub> H <sub>33</sub> N <sub>2</sub> O <sub>35</sub> S <sub>5</sub> Na <sub>3</sub> ] <sup>2-</sup>
IV	592.4	591.4	[C <sub>24</sub> H <sub>31</sub> N <sub>2</sub> O <sub>35</sub> S <sub>5</sub> Na <sub>5</sub> ] <sup>2-</sup>
	581.1	580.4	[C <sub>24</sub> H <sub>32</sub> N <sub>2</sub> O <sub>35</sub> S <sub>5</sub> Na <sub>4</sub> ] <sup>2-</sup>
	570.1	569.4	[C <sub>24</sub> H <sub>33</sub> N <sub>2</sub> O <sub>35</sub> S <sub>5</sub> Na <sub>3</sub> ] <sup>2-</sup>

located within the Chemistry Department at University of California at Santa Barbara. This instrument has been described in detail elsewhere.<sup>28</sup> The samples were made up to 50 µM in a solution of 50 : 49 : 1 methanol : water : acetic acid. Ions were created by negative electrospray ionisation and injected into a temperature regulated (298 K) drift cell pressurised with helium to 5 Torr. These ions drift under the influence of a weak electrostatic field and are retarded by collisions with the buffer gas. When they exit the cell, the oligosaccharides are analysed using a quadrupole mass spectrometer (Extrel) operating in scanning mode.

Mass spectra were obtained for each of the oligosaccharides, which were present in singly and doubly charged forms as partially sodiated species. The experimental and predicted masses for the major species observed for each oligosaccharide are listed in Table 1.

If an ion is pulsed into the cell, the quadrupole is then ‘parked’ on an ion of interest and its arrival time at the detector, relative to the start time of the pulse, is recorded. Arrival time distributions (ATDs) can then be collected at several drift voltages (90, 60, 45, 30 and 20 V) to obtain the reduced mobility ( $K_0$ ) of the ion, *via* a plot of arrival times *versus* the pressure of helium divided by the drift voltage. This mobility is used to determine the experimental collision cross section of the ion ( $\sigma$ ) according to eqn (1) below.<sup>29</sup>

$$K_0 = \frac{3e}{16N} \left( \frac{2\pi}{\mu k_B T} \right)^{1/2} \frac{1}{\sigma} \quad (1)$$

where  $N$  is the buffer gas number density, and  $\mu$  the reduced mass of ion and the buffer gas (here helium), and  $T$  is the temperature at which the measurements are taken.

Experimental cross sections are then compared to those obtained from candidate geometries modelled with the GLY-CAM force field (see below).

### Molecular modelling

**Parameterization of the AMBER force field.** We employed the Parm99 force field of AMBER7,<sup>30</sup> along with the GLY-CAM\_2000a<sup>31</sup> extension which includes parameters specific for carbohydrates. In addition, we have used parameters for sulfates and sulfamates according to Huige and Altona,<sup>32</sup> and introduced a new atom type, SO, for the sulfate group making it compatible with GLYCAM\_2000a parameters. The compatibility of parameters arising from the presence of the double-bond in the non-reducing terminal carbohydrate ring was also resolved. Some parameters for sulfate groups that were not available from the work of Huige and Altona<sup>32</sup> were approximated by those for phosphates from Parm99. Using the structures of oligosaccharides (I–IV) built by Xleap, partial

**Table 2** (a) Experimental data of ion mobility of the disaccharide ion **I**. (b) Experimental and theoretical cross sectional areas of oligosaccharides **I–IV**

(a) Fully sulfated disaccharide ( <b>I</b> )						
Pressure/bar		4.965	4.939	4.957	4.943	4.953
Voltage/V		91.39	61.20	45.69	30.70	20.13
$P/V$		0.054	0.081	0.108	0.161	0.246
ATD/ $\mu$ s	Monomer	385	490	600	810	1150
	Dimer	410	530	653	890	1280
	Trimer	485	645	805	1120	1625
$K_0/\text{cm}^2 \text{V}^{-1} \text{s}^{-1}$	Monomer		Dimer		Trimer	
			5.274		5.992	
$\sigma (\text{\AA}^2)$		4.024				
		132.1	201.6		266.8	

	(b) Compound					
	<b>I</b>			<b>II</b>	<b>III</b>	<b>IV</b>
$\sigma (\text{\AA}^2)$	Monomer	Dimer	Trimer			
Experimental	132.1	201.6	266.8	198.4	190.4	191.6
Calculated	134.8	191.7	250.2	204.1	190.3	191.8

atom charges were calculated with the RESP procedure (AMBER) using Gaussian98<sup>33</sup> and 6-31G\* basis set. The appropriate number of sodium counter ions were added to each oligosaccharide at random positions yielding the total charges of  $-1$  and  $-2$ , for the disaccharide monomer and tetrasaccharides, respectively. After optimization these ions occupy positions in the proximity of negatively charged groups as discussed later.

**Generation of candidate structures.** A simulated annealing protocol was used to generate 100 candidate structures for each oligosaccharide ion. The starting conformations were energy minimized during a 3 ps steepest descent step followed by a gradient method of 0.5 ns. Optimized structures were subjected to 30 ps of molecular dynamics at 800 K with constrained dynamics of bonds involving H-atoms.<sup>34</sup> The system was then cooled to 0 K during a period of 10 ps using ten cooling steps of 80 K and energy minimized in the same way as the initial energy minimization was carried out. Candidate conformations obtained in this way are used as inputs for each subsequent round of the simulated annealing.

**Calculation of theoretical cross sections.** The ions were modelled using the projection approximation method as a

collection of overlapping hard spheres with radii equal to hard sphere collision distances, corrected for collision temperature.<sup>13</sup> Orientationally-averaged, geometric cross sections were determined by averaging the geometric cross sections over all possible collision geometries. The reported theoretical cross-sections (Table 2) were obtained by averaging the cross sections of the 10% lowest energy structures.

**Calculation of  $\Phi$ ,  $\Psi$  energy maps of disaccharide segments found in compounds **I–IV**.** The relative orientation of individual monosaccharide rings is described by the dihedral angles  $\Phi(\text{H}_1\text{---C}_1\text{---O---C}_4)$  and  $\Psi(\text{C}_1\text{---O---C}_4\text{---H}_4)$ . These angles were restrained in  $10^\circ$  steps between  $-180^\circ$  and  $180^\circ$  and the structures were energy minimized during a 3 ps steepest descent step followed by a gradient method of 0.5 ns, using the force field described above. The calculations were performed in vacuum and in the absence of  $\text{Na}^+$  ions. The non-bonded cut-off value was set to 999  $\text{\AA}$  and a distance-dependant dielectric constant was used. For  $\Delta\text{UA}(2\text{S})$  and  $\text{IdoA}(2\text{S})$  residues (rings D and B) two ( ${}^1\text{H}_2$  and  ${}^2\text{H}_1$ ) and three ( ${}^1\text{C}_4$ ,  ${}^4\text{C}_1$  and  ${}^2\text{S}_0$ ) starting conformations were used, respectively. These conformations were not fixed during the calculations, although they did not change. Only the map that produced the lowest energy minima is shown in Fig. 7. The resulting  $\Phi$ ,  $\Psi$  maps were drawn using ten isoenergy contours in 1 kcal mol<sup>-1</sup> steps above the global minimum.

### 3. Results

For this study we have prepared one disaccharide (**I**) and three tetrasaccharides (**II–IV**) (Fig. 1b), as described in the ESI†. These were the predominant di- and tetra-saccharides excised from heparin by the action of heparinase **I**. Disaccharide **I** and tetrasaccharide **II** are fully sulfated species possessing three and six sulfate/sulfamate groups, respectively. Their structures were therefore obvious from disaccharide analyses (*i.e.*  $[\Delta\text{UA}(2\text{S})\text{-GlcNS}(6\text{S})]_{1-2}$ ), but were confirmed by NMR and MS. Two lesser sulfated tetrasaccharides (**III** and **IV**) were also obtained that possessed asymmetric disaccharide compositions. In these cases NMR was used to assign the absolute sequence. In tetrasaccharide **III**, position  $\text{C}_6$  of ring A is not sulfated (*i.e.* GlcNS). In the case of tetrasaccharide **IV**, ring B is a non-sulfated GlcA rather than a 2-O-sulfated IdoA as in **II** and **III**. All oligosaccharides contain a  $\text{C}_4\text{---C}_5$  double bond in the non-reducing uronate ring D resulting from the enzymatic lyase cleavage that was used to excise the oligosaccharides from the heparin polysaccharide. At the reducing end monosaccharide the  $\alpha$  anomers are the prevailing species in solution ( $\alpha : \beta = 9 : 1$ , as determined by NMR). We have not found any significant difference in the theoretical cross sections between these two ( $\alpha$  or  $\beta$ ) forms. This is in agreement with the experimental ATDs

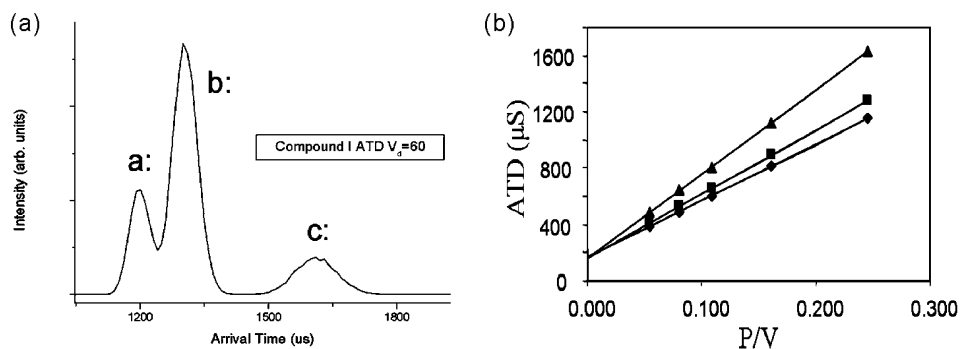


**Fig. 2** (a) Arrival time distribution for the 642.4  $m/z$  ion of disaccharide **I**. An electric gradient of 60 V was used. The peaks labelled a–c correspond to a monomer, dimer and trimer of **I**, respectively. (b) Determination of experimental ion mobility,  $K$ , for three arrival time distributions observed for disaccharide monomer ( $\blacklozenge$ ), dimer ( $\blacksquare$ ) and trimer ( $\blacktriangle$ ) of **I**. (Data from Table 2(a))

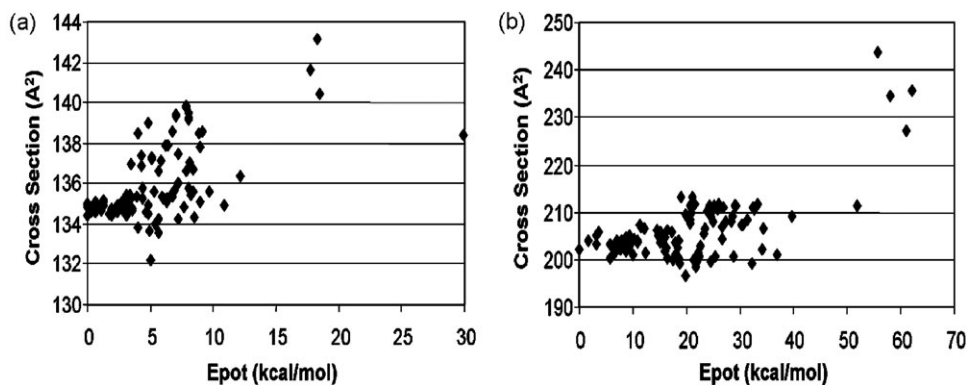


**Fig. 3** Theoretical cross sections of 100 candidate structures of (a) disaccharide **I** and (b) tetrasaccharide **II** ions as a function of the potential energy.

that did not show any indications of separate peaks attributable to different anomeric forms. Only  $\alpha$  anomeric configurations of the reducing end monosaccharides are therefore considered below.

### Ion mobility mass spectrometry

We have obtained high quality IM-MS data from one disaccharide and three tetrasaccharide samples. The ions generated from disaccharide **I** showed three distinct arrival distribution times (Fig. 2a) at an apparent mass of 642.4  $m/z$ . Early in our data analysis it became clear that the species with longer ATDs could not be reproduced by considering only a monomeric ion ( $[\text{C}_{12}\text{H}_{15}\text{NO}_{19}\text{S}_3\text{Na}_3]^-$ ) and that these correspond to a dimer and trimer of **I** ( $[\text{C}_{12}\text{H}_{15}\text{NO}_{19}\text{S}_3\text{Na}_3]_2^{2-}$  and  $[\text{C}_{12}\text{H}_{15}\text{NO}_{19}\text{S}_3\text{Na}_3]_3^{3-}$ , respectively) that were formed in the collision cell. The ion mobility,  $K$ , was obtained *via* a plot of arrival times *versus* the pressure of helium divided by the drift voltage (Fig. 2b). Using these values, the experimental cross-sections were calculated using eqn (1) (Table 2).

The ions generated using tetrasaccharides **II–IV** were principally monomeric and corresponded to the following species:  $[\text{C}_{24}\text{H}_{30}\text{N}_2\text{O}_{38}\text{S}_6\text{Na}_6]^{2-}$  (**II**, 642.4  $m/z$ ) and  $[\text{C}_{24}\text{H}_{31}\text{N}_2\text{O}_{35}\text{S}_5\text{Na}_5]^{2-}$  (**III**, **IV**, 591.4  $m/z$ ) (Table 1). Their arrival time distributions were analyzed as explained above for the disaccharide, and the resulting experimental cross-sectional areas are summarized in Table 2.

The number of Na atoms lost during the ionization process (one for the disaccharide and two for tetrasaccharides) corresponds exactly to the number of carboxyl groups, implying a stronger affinity of sulfate and sulfamate groups for sodium compared with carboxyl groups.

### Molecular modelling

Candidate structures of oligosaccharides and their oligomers were obtained by molecular modelling, as detailed in the Experimental section. For each of these structures the theoretical cross-sections were calculated (Fig. 3) as explained in the Experimental section. The theoretical cross-sections, reported in Table 2, were obtained by averaging the cross-sections of the 10% lowest energy structures.

The agreement between the experimental and theoretical cross-sections is very good. For monomers the differences were <2.1%, while for oligomers they were <6.2%

### Conformations of ions generated from oligosaccharides I–IV

The ten lowest energy structures of the monomeric disaccharide **I** ion,  $[\text{C}_{12}\text{H}_{15}\text{NO}_{19}\text{S}_3\text{Na}_3]^-$ , differed only slightly in the orientation of their functional groups (Fig. 4)

The  $\Delta\text{UA}$  ring (D) was always found in the  ${}^1\text{H}_2$  conformation while the glucosamine residue (ring A) invariably occupied

the  ${}^4\text{C}_1$  conformation. Two  $\text{Na}^+$  ions were coordinated by two sulfate groups, while the third was positioned between the sulfamate and carboxyl groups. As a general feature of all structures we simulated, the  $\text{Na}^+$  ions were found between 2.2 and 2.9 Å from oxygen atoms of at least two sulfate, sulfamate or carboxyl groups.

Although the prevailing conformations of rings D and A in the dimer and the trimer were the same as observed for the monomer disaccharide ( ${}^1\text{H}_2$  and  ${}^4\text{C}_1$ ), other forms ( $\text{B}_{3,0}$  for ring D and  ${}^1\text{S}_5$ ,  ${}^5\text{S}_3$  for ring A) were also found. We attribute the existence of these forms to the presence of Coulombic interactions between the  $\text{Na}^+$  ions and negatively charged groups causing distortions of the ring conformations. In all dimers the  $\text{Na}^+$  cations were simultaneously coordinated to both monomer units. In the trimers all  $\text{Na}^+$  ions were coordinated by at least two monomers, while some showed simultaneous interactions with all three monomers. In addition, several hydrogen bonds were observed between some monomers using the criterion for the distance between the atom, D<sub>3</sub>, carrying hydrogen donor and oxygen acceptor (A) was <3 Å and the angle |D–H–A| was <20° (Fig. 5).

An example of the structures of the tetrasaccharide ions is given in Fig. 6, which shows that obtained for the fully sulfated tetrasaccharide, **II**.

The overlay of the lowest energy structures of the tetrasaccharide ions showed some heterogeneity in the conformation of individual monosaccharide rings. In particular, both  ${}^1\text{H}_2$  and  ${}^2\text{H}_1$  forms were present in ring D. Ring A also showed, in addition to a  ${}^4\text{C}_1$  conformation, both boat and skew boat forms. The IdoA (ring B) consistently occupied a  ${}^4\text{C}_1$  conformation, although the solution structure of **II** indicates the prevalence of the  ${}^2\text{S}_0$  form.<sup>35</sup> Calculations performed on this tetrasaccharide with the Born Solvent model<sup>36</sup> resulted in interconversion between the usual  ${}^1\text{C}_4$  and  ${}^2\text{S}_0$  forms for the IdoA ring. This indicates that the  ${}^4\text{C}_1$  is specific to the gas phase rather than the AMBER force-field we have used. For a monosaccharide our IM-MS instrumentation will not

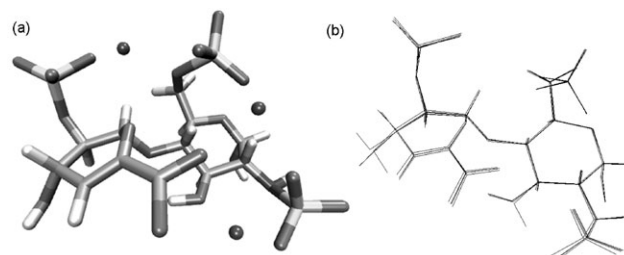


**Fig. 4** Lowest energy structures of the  $[\text{C}_{12}\text{H}_{15}\text{NO}_{19}\text{S}_3\text{Na}_3]^-$  disaccharide **I** ion. (a) A typical structure of **I**.  $\text{Na}^+$  is shown as spheres. (b) Overlay of the ten lowest energy structures. The structures were generated using MolMol<sup>43</sup> and are oriented as shown in Fig. 1.

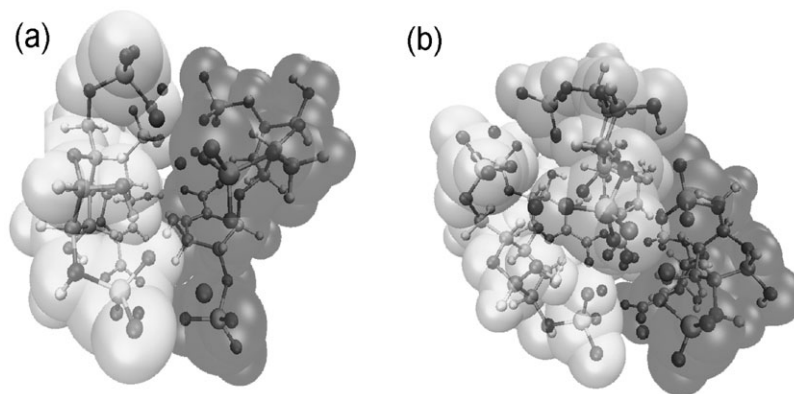


**Fig. 5** Representative structures of (a)  $[C_{12}H_{15}NO_{19}S_3Na_3]_2^{2-}$  and (b)  $C_{12}H_{15}NO_{19}S_3Na_3]_3^{3-}$  ions corresponding to the dimer and trimer of **I**. The structures were generated with VMD.<sup>42</sup> Individual monomers are highlighted using van der Waals radii of their atoms.

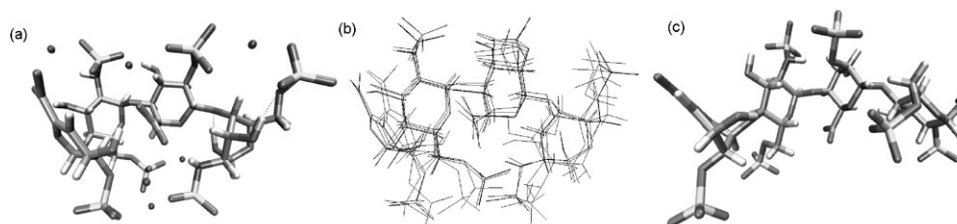


**Fig. 6** Fully sulfated tetrasaccharide, **II**. (a) Representative structures of  $C_{24}H_{30}N_2O_{38}S_6Na_6]^{2-}$  ion. (b) overlay of the five lowest energy structures (c) Crystal structure of **II** in complex<sup>37</sup> with bFGF. The structures are oriented as shown in Fig. 1.

distinguish between the three forms of IdoA monosaccharide, as their theoretical cross sections differ by  $<2\%$  (data not shown). Nevertheless, in the context of a larger molecule different conformations of IdoA monosaccharide will influence the overall shape of the molecule and therefore be indirectly traceable *via* molecular modelling.

A notable feature of the lowest energy structures of the tetrasaccharide ions is their “compact” shape (Fig. 6b), which differs from the more extended conformation observed in the X-ray structure<sup>35</sup> of **II** complexed with basic fibroblast growth factor (bFGF) (Fig. 6c). The theoretical cross section of the X-ray structure ( $231.8 \text{ \AA}^2$ ) is substantially larger than that of

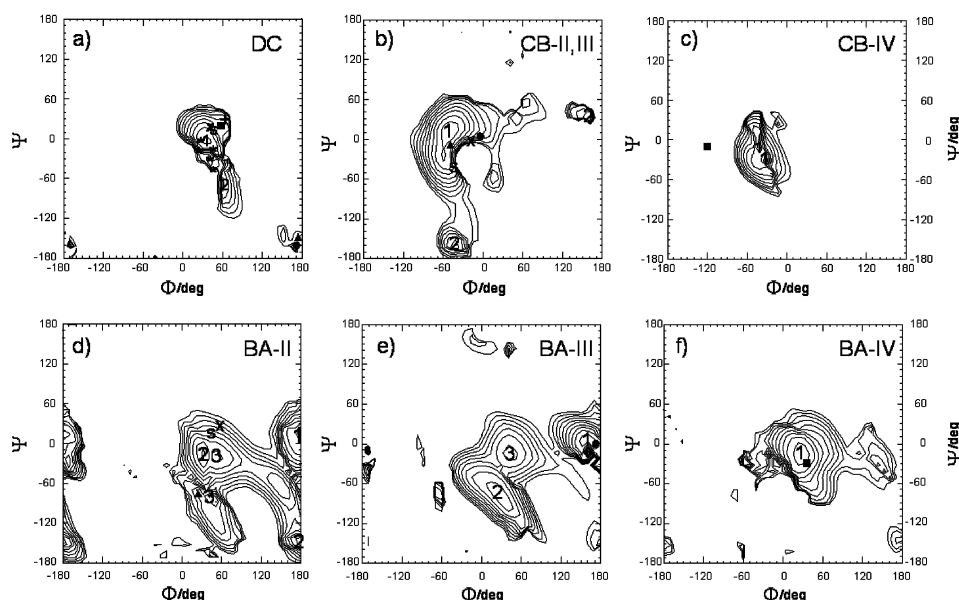


**Fig. 7**  $\Phi, \Psi$  energy maps calculated as detailed in the Material and Methods section for disaccharide segments of oligosaccharides **I-IV**. The following conformations of individual rings were considered: DC:  ${}^1H_2\text{-}{}^4C_1$ ; CB and BA:  ${}^4C_1\text{-}{}^4C_1$ . Ten isoenergy contours are drawn by interpolation of  $1 \text{ kcal mol}^{-1}$  above the global minimum. The conformation found for disaccharide ions are marked by + (monomer) and \* (dimer and trimer). Conformations found for tetrasaccharide ions **II, III** and **IV** are labelled using  $\blacktriangle$ ,  $\bullet$  and  $\blacksquare$ , respectively. The dihedral angles found in the solution structures of the tetrasaccharide **II** are marked by x and s, respectively. (a) CD disaccharide segments. The energy minima labelled as 1 and 2 are separated by  $4 \text{ kcal mol}^{-1}$ . (b) Rings C and B in tetrasaccharide ions **II, III**. The energy minima 1 and 2 are separated by  $3 \text{ kcal mol}^{-1}$ . (c) Rings C and B in the tetrasaccharide ion **IV**. (d) Rings B and A in tetrasaccharide ion **II**. The energy minima marked as 1, 2 and 3 are separated by  $1 \text{ kcal mol}^{-1}$ . (e) Rings B and A in tetrasaccharide ion **III**. The energy minima 1 and 2, and 1 and 3 are separated by 1 and  $3 \text{ kcal mol}^{-1}$ , respectively. (f) Rings B and A in tetrasaccharide ion **IV**.

the corresponding low energy structures in the gas phase (204.1 Å<sup>2</sup>). Clearly, the value obtained from our calculated structures is much closer to the experimental value of 198 Å<sup>2</sup>. Even better agreement between the theoretical and experimental cross sections was observed for tetrasaccharide ions **III** and **IV** (Table 2), indicating that our model structures are a true representation of their gas phase conformation. The reasons why the gas-phase conformations are more compact are explained in the discussion.

The overall shape of an oligosaccharide molecule is, to a large extent, determined by the conformation of the glycosidic linkage. In the following we therefore discuss the conformations of the glycosidic linkages of the gas phase oligosaccharide ions **I–IV**. We also turn our attention to Na<sup>+</sup> ions and their effect on the gas phase conformation of heparin-derived oligosaccharide ions.

## Discussion

Compact structures of gas phase ions have been observed in an IM-MS study of neutral, sodiated carbohydrates,<sup>38</sup> and recent work by Hill *et al.*<sup>39</sup> reports the use of atmospheric pressure ion mobility to separate sodiated di and tri-saccharides. We show here that interactions of Na<sup>+</sup> with negatively charged sulfates, sulfamates and carboxyl groups resulted in the formation of higher oligomers of disaccharide ions; aggregation was not reported by Hill. Are these interactions also responsible for the “compact” shape of the tetrasaccharide ions that reproduced so well our IM-MS data? Or is it our force field that favours certain conformations around the glycosidic linkage leading to compact structures? In order to answer these questions we have calculated structures of three disaccharide segments, contained in each of the tetrasaccharides **II–IV**, in the absence of Na<sup>+</sup>. The results of these calculations are presented in the form of  $\Phi$ ,  $\Psi$  energy maps (Fig. 7), that are also used to indicate the dihedral angles observed in our modelled structures of the gas phase ions (Tables 3 and 4), and also those found in the solution<sup>35</sup> and solid state structures.<sup>37</sup>

For these calculations we have used conformations of individual rings corresponding to the most populated species found in our modelled gas phase structures in the presence of Na<sup>+</sup>.

Starting from the non-reducing end of the molecule we first examine the DC disaccharide segment. The dihedral angles observed for the monomeric disaccharide ion [C<sub>12</sub>H<sub>15</sub>NO<sub>19</sub>S<sub>3</sub>Na<sub>3</sub>]<sup>−</sup> deviate up to +30° on both angles from the deepest minimum of the  $\Phi$ ,  $\Psi$  map. Deviations in the opposite direction, and of up to −45° in the  $\Psi_{DC}$  angle, were observed for dimeric and trimeric disaccharide ions. The largest differences were, however, observed for the DC linkages in the tetrasaccharide ions **II** and **III**, corresponding to the existence of anti conformers (symbols ▲ and ● in Fig. 7a). This region of the  $\Phi$ ,  $\Psi$  map was not particularly energetically favoured in the absence of the sodium, but presumably became stabilized by the Na<sup>+</sup> cations interacting with both D and

**Table 3** Structural parameters of the lowest energy conformers of disaccharide **I** and its oligomers

	Ring D	Ring A	$\Phi$	$\Psi$
Monomer	<sup>1</sup> H <sub>2</sub>	<sup>4</sup> C <sub>1</sub>	64	28
X-Ray <sup>37</sup>	<sup>1</sup> H <sub>2</sub>	<sup>4</sup> C <sub>1</sub>	42.3	18.3
Solution <sup>35</sup>	<sup>1</sup> H <sub>2</sub>	<sup>4</sup> C <sub>1</sub>	45.7	13.2
Dimer	<sup>1</sup> H <sub>2</sub>	<sup>1</sup> S <sub>5</sub>	41	−30
	<sup>1</sup> H <sub>2</sub> /B <sub>3,0</sub>	<sup>4</sup> C <sub>1</sub>	45	−16
Trimer	<sup>1</sup> H <sub>2</sub>	<sup>4</sup> C <sub>1</sub>	26	−18
	<sup>1</sup> H <sub>2</sub> /B <sub>3,0</sub>	<sup>4</sup> C <sub>1</sub>	27	−4
	<sup>1</sup> H <sub>2</sub> /B <sub>3,0</sub>	<sup>5</sup> S <sub>3</sub>	45	−47

**Table 4** Structural parameters of the lowest energy conformers of the tetrasaccharide ions **II**, **III** and **IV**

Dihedral angle	Crystal structure <sup>37</sup>	Solution structure <sup>35</sup>	<b>II</b>	<b>III</b>	<b>IV</b>
$\Phi_{DC}$	42.3	45.7	175.8	172.0	61.0
$\Psi_{DC}$	18.3	13.2	−149.4	−159.7	20.0
$\Phi_{CB}$	−18.5	−43.3	−48.8	−3.9	−129.8
$\Psi_{CB}$	−3.5	−42.2	−10.8	5.0	−11.2
$\Phi_{BA}$	57.0	45.2	25.5	176.6	34.7
$\Psi_{BA}$	25.1	15.0	−78.5	0.8	−30.0

A rings. The corresponding dihedral angles observed in the X-ray and solution structures were close to the minimum of the  $\Phi$ ,  $\Psi$  map.

The next two disaccharide segments can only be examined in the context of the tetrasaccharides. Considering tetrasaccharide ions **II** and **III** first, we note that the CB segments are structurally identical in these two compounds and that the dihedral angles of the tetrasaccharide ion **II** are close to the minimum of the  $\Phi$ ,  $\Psi$  map (Fig. 7b). However, in compound **III** the  $\Phi_{CB}$  angle differs by 45°. It is possible that this difference is a consequence of a different conformation found in the BA disaccharide segment of ions **II** and **III** (see Table 4 and Fig. 7d,e), and it is therefore not possible to attribute this difference solely to effects of the Na<sup>+</sup> ions. On the other hand, a large difference in the dihedral angle  $\Phi_{CB}$  (80°) was observed between the sodium-free disaccharide segment and the gas phase conformation of tetrasaccharide ion **IV** (Fig. 7c). The latter clearly occupies a high energy region of the  $\Phi$ ,  $\Psi$  map.

Because of the differences in the primary sequence of tetrasaccharides **II–IV**, three separate cases must be considered when analysing the BA disaccharide segment. In compound **II** the gas phase ion structure is not found in the global minimum ( $\Phi$ ,  $\Psi$ ) = (180°, 10°), but occupies a secondary minimum (+2 kcal mol<sup>−1</sup>) with coordinates (26, −79). This conformation also differs by ~105° in the  $\Psi_{AB}$  angle from the X-ray and solution structures. Ions **III** and **IV** on the other hand show conformations coinciding with the global minima of the sodium-free disaccharide segments (Fig. 7e,f).

In summary, the analysis presented above showed that considerable differences exist between the structures calculated in the presence or absence of Na<sup>+</sup>. It appears that sodium atoms play an important role in stabilising the gas phase conformation of ions, leading to the appearance of “compact” structures of tetrasaccharide ions. In these structures rings A and D are brought close to each other and bridged by sodium cations. In order to accommodate such conformations, some glycosidic linkages adopt conformations that differ from those calculated for the sodium free disaccharide segments, or those observed in the solution or X-ray structures of tetrasaccharide **II**.

Let us now take a closer look at the conformations of the gas phase structures of the three tetrasaccharides **II–IV** as described by the dihedral angles along individual glycosidic linkages (Table 4). It can be seen that a small change in the primary structure can lead to different conformations. For example, tetrasaccharides **II** and **III**, which differ only in one sulfate at position A6, show markedly different conformations along the CB and BA glycosidic linkages. Similarly, GlcA/IdoA isomerism (compounds **II** and **IV**) resulted in very different conformations. This is an interesting result showing that, at least in the gas phase, differences in the primary structures of HS/heparin sequences can lead to different conformations. It is also possible that the conformations revealed by IM-MS exist transiently in solution generating short-lived “kinks and turns” in otherwise regular, helical structures of HS/heparin.<sup>9</sup>

Na<sup>+</sup> ions interact differently with the negatively charged groups of glycosaminoglycans in solution and in the gas phase. In solution the hydrated sodium counterions are delocalized in the volume around the polyanion,<sup>40</sup> while in the gas phase the Na<sup>+</sup> cations are localized near several negatively charged groups as seen in this study. This effect will lessen the Coulombic repulsion that isolated sulfate groups would impart on each other, and has the effect of ‘tightening’ the structures. This explains the lower cross section obtained in the gas-phase compared with that from X-ray data. By using the ionization conditions as described by Zai and Costello<sup>41</sup> it may be possible to obtain Na<sup>+</sup>-free ions of heparin-derived oligosaccharides for ion-mobility studies that would bear a closer resemblance to conditions seen in solution. In particular, this may be possible for low sulfated HS species which so far have received much less attention compared with highly sulfated domains. Although the low sulfated species are unlikely to be involved in protein recognition, they may well be the source of flexibility in HS/heparin polymers and this could be probed by MS-IM. A significant advantage of IM-MS over other biophysical methods applicable to conformational studies of biomolecules is that the ion-mobility experiments can be performed at near liquid nitrogen temperatures. Under these conditions different conformers can potentially be separated providing they exhibit distinct cross sectional areas. Other methods, such as NMR, can only report on the time-averaged structures.

## Conclusions

We have performed a conformational analysis of ions of heparin-derived oligosaccharides using ion-mobility mass spectrometry and molecular modelling. Negative mode electrospray ionisation has produced singly (disaccharide) and doubly charged (tetrasaccharide) ions containing three and six Na<sup>+</sup> ions, respectively. A good agreement was obtained between the experimental and theoretical cross sections. The latter were obtained using modelled structures generated by the AMBER-based force field. Analysis of the data shows that the sodium cations play a major role in stabilizing the ions in the gas phase. This was seen in the formation of oligomers of the disaccharide and ‘compact’ structures of tetrasaccharide ions. Interestingly, the conformations of the three tetrasaccharides, differing by relatively small changes in primary structure, were significantly different.

## Acknowledgements

We thank Professor Mike Bowers (University of California at Santa Barbara) for use of his Ion Mobility Apparatus. The EPSRC are thanked for part funding these studies through the award of an Advanced Research Fellowship to PEB. Lan Jin acknowledges the support of the ORS scheme and that of the University of Edinburgh. Malcolm Lyon and Jon A. Deakin are supported by a CRUK Programme Grant.

## References

- M. Bernfield, M. Gotte, P. W. Park, O. Reizes, M. L. Fitzgerald, J. Lincecum and M. Zako, *Annu. Rev. Biochem.*, 1999, **68**, 729–777.
- M. Bernfield, R. Kokenyesi, M. Kato, M. T. Hinkes, J. Spring, R. L. Gallo and E. J. Lose, *Annu. Rev. Cell Biol.*, 1992, **8**, 365–393.
- L. Kjellen and U. Lindahl, *Annu. Rev. Biochem.*, 1991, **60**, 443–475.
- K. J. Murphy, C. L. R. Merry, M. Lyon, I. S. Roberts, J. E. Thompson and J. T. Gallagher, *J. Biol. Chem.*, 2004, **279**, 27239–27245.
- B. Casu and U. Lindahl, *Adv. Carbohydr. Chem. Biochem.*, 2001, **57**, 159–206.
- E. Conrad, *Heparin Binding Proteins*, Academic Press, San Diego, 1998.
- (a) J. Schlessinger, A. N. Plotnikov, O. A. Ibrahim, A. V. Eliseenkova, B. K. Yeh, A. Yaron, R. J. Linhardt and M. Mohammadi, *Mol. Cell*, 2000, **6**, 743–750; (b) L. Pellegrini, D. F. Burke, F. V. Delft, B. Mulloy and T. L. Blundell, *Nature*, 2000, **407**, 1029–1034; (c) I. Capila, M. J. Hernáiz, Y. D. Mo, T. R. Mealy, B. Campos, J. R. Dedman, R. J. Linhardt and B. A. Seaton, *Structure*, 2001, **9**, 57–64; (d) A. D. DiGabriele, I. Lax, D. I. Chen, C. M. Svahn, M. Jaye, J. Schlessinger and W. A. Hendrickson, *Nature*, 1998, **393**, 812–817.
- E. D. T. E. Atkins and I. A. Nieduszynski, *Adv. Exp. Med. Biol.*, 1975, **52**, 19.
- B. Mulloy, M. J. Forster and C. Jones, *Biochem. J.*, 1993, **293**, 849.
- D. Spillmann, D. Witt and U. Lindahl, *J. Biol. Chem.*, 1998, **273**, 15487.
- I. Capila, M. J. Hernaiz, Y. D. Mo, T. R. Mealy, B. Campos, J. R. Dedman, R. J. Linhardt and B. A. Seaton, *Structure*, 2001, **9**, 57.
- A. K. Powell, E. A. Yates, D. G. Ferning and J. E. Turnbull, *Glycobiology*, 2004, **14**, 17R–30R.
- T. Wyttenback and M. T. Bowers, *Top. Curr. Chem.*, 2003, **255**, 207–232.
- M. F. Jarrold, *Ann. Rev. Phys. Chem.*, 2000, **51**, 179–207.
- R. H. H. van den Heuvel and J. R. Albert Heck, *Curr. Opin. Chem. Biol.*, 2004, **8**, 519–526.
- J. Gidden, A. Ferzoco, E. S. Baker and M. T. Bowers, *J. Am. Chem. Soc.*, 2004, **126**, 15132–15140.
- Z. Shriver, R. Raman, G. Venkataraman, K. Drummond, J. Turnbul, T. Toida, R. Linhardt, K. Biemann and R. Sasisekharan, *Biochemistry*, 2000, **39**, 10359–10364.
- R. M. Pope, C. S. Raska, S. C. Thorp and J. Liu, *Glycobiology*, 2001, **11**, 505–513.
- G. Venkataraman, Z. Shriver, R. Raman and R. Sasisekharan, *Science*, 1999, **286**, 537–542.
- B. Kuberan, M. Lech, L. Zhang, Z. L. Wu, D. L. Beeler and R. D. Rosenberg, *J. Am. Chem. Soc.*, 2002, **124**, 8707–8718.
- H. Desaire and J. A. Leary, *J. Am. Soc. Mass Spectrom.*, 2000, **11**, 916–920.
- O. M. Saad and J. A. Leary, *J. Am. Soc. Mass Spectrom.*, 2004, **15**(9), 1274–1286.
- O. M. Saad and J. A. Leary, *Anal. Chem.*, 2003, **75**(13), 2985–2995.
- J. Zai and C. E. Costello, *Anal. Chem.*, 2003, **75**(10), 2445–2455.
- K. Giles, S. D. Pringle, K. R. Worthington, D. Little, J. L. Wildgoose and R. H. Bateman, *Rapid Commun. Mass Spectrom.*, 2004, **18**(20), 2401–2414.
- P. Dugourd, R. R. Hudgins, D. E. Clemmer and M. F. Jarrold, *Rev. Sci. Instrum.*, 1997, **68**(2), 1122–1129.
- J. Jiménez-Barbero and T. Peters, *NMR Spectroscopy of Glycoconjugates*, WILEY-VCH, 2003.
- T. Wyttenbach, P. R. Kemper and M. T. Bowers, *Int. J. Mass Spectrom.*, 2001, **212**(1–3), 13–23.
- E. A. Mason and E. W. McDaniel, *Transport Properties of Ions in Gases*, Wiley, New York, 1988.
- D. A. Case, D. A. Pearlman, J. W. Caldwell, T. E. Cheatham III, J. Wang, W. S. Ross, C. L. Simmerling, T. A. Darden, K. M. Merz, R. V. Stanton, A. L. Cheng, J. J. Vincent, M. Crowley, V. Tsui, H. Gohlke, R. J. Radmer, Y. Duan, J. Pitera, I. Massova, G. L. Seibel, U. C. Singh, P. K. Weiner and P. A. Kollman, *AMBER 7*, University of California, San Francisco, 2002.
- Dr Woods website, [http://glycam.cerc.uga.edu/glycam/glycam\\_parameters.html](http://glycam.cerc.uga.edu/glycam/glycam_parameters.html).
- C. J. M. Huige and C. Altona, *J. Comp. Chem.*, 1995, **16**, 56–79.
- M. J. Frisch, G. W. Trucks, H. B. Schlegel, G. E. Scuseria, M. A. Robb, J. R. Cheeseman, V. G. Zakrzewski, J. A. Montgomery Jr., R. E. Stratmann, J. C. Burant, S. Dapprich, J. M. Millam, A. D. Daniels, K. N. Kudin, M. C. Strain, O. Farkas, J. Tomasi, V. Barone, M. Cossi, R. Cammi, B. Mennucci, C. Pomelli, C. Adamo, S. Clifford, J. Ochterski, G. A. Petersson, P. Y. Ayala, Q. Cui, K. Morokuma, D. K. Malick, A. D. Rabuck, K. Raghavachari, J. B. Foresman, J. Cioslowski, J. V. Ortiz, B. B. Stefanov, G. Liu, A. Liashenko, P. Piskorz, I. Komaromi, R. Gomperts, R. L. Martin, D. J. Fox, T. Keith, M. A. Al-Laham, C. Y. Peng, A. Nanayakkara, C. Gonzalez, M. Challacombe, P. M. W. Gill, B. Johnson, W. Chen, M. W. Wong, J. L. Andres, C. Gonzalez, M. Head-Gordon, E. S. Replogle, and J. A. Pople, *GAUSSIAN 98, (Revision A.6)*, Gaussian, Inc, Pittsburgh PA, 1998.
- J.-P. Ryckaert, G. Ciccotti and H. J. C. Berendsen, *J. Comput. Phys.*, 1977, **23**, 327–341.
- D. Mikhailov, K. H. Mayo, I. R. Vlahov, T. Toida, A. Pervin and R. J. Linhardt, *Biochem. J.*, 1996, **318**, 93–102.
- D. Bashford and D. A. Case, *Annu. Rev. Phys. Chem.*, 2000, **51**, 129–152.
- S. Faham, R. E. Hileman, J. R. Fromm, R. J. Linhardt and D. C. Rees, *Science*, 1996, **271**, 1116–1120.

- 
- 38 S. Lee, T. Wyttenbach and M. T. Bowers, *Int. J. Mass Spectrom.*, 1997, **167**, 605–614.
- 39 B. H. Clowers, P. Dwivedi, W. E. Steiner and H. H. Hill Jr., *J. Am. Soc. Mass Spectrom.*, 2005, **16**, 660–669.
- 40 D. L. Rabenstein, J. M. Robert and J. Peng, *Carbohydr. Res.*, 1995, **278**(2), 239–256.
- 41 J. Zaia and C. E. Costello, *Anal. Chem.*, 2001, **73**, 233–239.
- 42 W. Humphrey, A. Dalke and K. Schulten, *J. Mol. Graphics*, 1996, **14**, 33–38. VMD -Visual Molecular Dynamics, <http://www.ks.uiuc.edu/Research/vmd/>.
- 43 R. Koradi, M. Billeter and K. Wüthrich, *J. Mol. Graphics*, 1996, **14**, 51–55. MOLMOL: a program for display and analysis of macromolecular structures.